

BitGNN: Unleashing the Performance Potential of Binary Graph Neural Networks on GPUs

Jou-An Chen

North Carolina State University
Raleigh, NC, USA
jchen73@ncsu.edu

Hsin-Hsuan Sung

North Carolina State University
Raleigh, NC, USA
hsung2@ncsu.edu

Xipeng Shen

North Carolina State University
Raleigh, NC, USA
xshen5@ncsu.edu

Sutanay Choudhury

Pacific Northwest National
Laboratory
Richland, WA, USA
Sutanay.Choudhury@pnnl.gov

Ang Li

Pacific Northwest National
Laboratory
Richland, WA, USA
ang.li@pnnl.gov

ABSTRACT

Recent studies have shown that Binary Graph Neural Networks (GNNs) are promising for saving computations of GNNs through binarized tensors. Prior work, however, mainly focused on algorithm designs or training techniques, leaving it open to how to materialize the performance potential on accelerator hardware fully. This work redesigns the binary GNN inference backend from the efficiency perspective. It fills the gap by proposing a series of abstractions and techniques to map binary GNNs and their computations best to fit the nature of bit manipulations on GPUs. Results on real-world graphs with GCNs, GraphSAGE, and GraphSAINT show that the proposed techniques outperform state-of-the-art binary GNN implementations by 8-22X with the same accuracy maintained. BitGNN code is publicly available.¹.

CCS CONCEPTS

- Computing methodologies → Neural networks; Massively parallel algorithms;
- Computer systems organization → Single instruction, multiple data.

KEYWORDS

graph neural networks, binarized GNN, bit manipulation, GPU, sparse matrix

ACM Reference Format:

Jou-An Chen, Hsin-Hsuan Sung, Xipeng Shen, Sutanay Choudhury, and Ang Li. 2023. BitGNN: Unleashing the Performance Potential of Binary Graph Neural Networks on GPUs. In *International Conference on Supercomputing (ICS '23), June 21–23, 2023, Orlando, FL, USA*. ACM, New York, NY, USA, 13 pages. <https://doi.org/10.1145/3577193.3593725>

¹<https://github.com/PICTureRG/BitGNN>

Permission to make digital or hard copies of all or part of this work for personal or classroom use is granted without fee provided that copies are not made or distributed for profit or commercial advantage and that copies bear this notice and the full citation on the first page. Copyrights for components of this work owned by others than the author(s) must be honored. Abstracting with credit is permitted. To copy otherwise, or republish, to post on servers or to redistribute to lists, requires prior specific permission and/or a fee. Request permissions from permissions@acm.org.

ICS '23, June 21–23, 2023, Orlando, FL, USA

© 2023 Copyright held by the owner/author(s). Publication rights licensed to ACM.
ACM ISBN 979-8-4007-0056-9/23/06...\$15.00
<https://doi.org/10.1145/3577193.3593725>

1 INTRODUCTION

Recent years have witnessed a rapidly increasing adoption of Graph Neural Networks (GNNs) in various domains, from social networks [1] to bioinformatics [2], computational chemistry [3, 4], 3D computer vision [5, 6], and so on. GNN allows the linear and non-linear transformations of Neural Networks to work directly on graphs. By seamlessly integrating both the graph structure and node/edge features into the modeling, GNN is a natural fit for graph-based problems. Numerous studies [7–12] on graph-based classification and prediction have reported significantly better results achieved through GNNs than traditional methods.

Because real-world graphs are often large, GNN inference is often time-consuming and space-hungry, frequently exceeding the capacity of the storage or memory and the desirable latency. Inspired by the binarization (i.e., quantization to the 1-bit extreme) for ordinary deep neural networks [13–17], an emerging effort is to investigate the potential of GNN binarization. By converting each value in the activation maps, weights, and/or adjacency matrices into a single bit (sometimes through matrix factorizations), GNN binarization can significantly reduce the space demands and computation amounts.

The continuous research in the recent several years on GNN binarization have achieved some remarkable advances [18–21]. For instance, we have seen the reduction of binarization-caused accuracy loss from 16% to less than 5%. The loss of accuracy can be controlled within a small percentage on various graphs and architectures while giving significant theoretical reductions in the number of computations and memory usage. Nevertheless, how to turn the potential into full speedups and memory savings on real machines remains an open question. For example, based on a theoretical analysis, the authors of a recent study [18] on binary GNNs report ~47X potential savings of computations and ~30X possible memory footprint reduction. Still, their experiments show no speedups or memory savings over the original non-binarized GNN.

Existing work on binary GNNs mainly focuses on *algorithm-level* improvement on network architectures [18–20] or training techniques [18, 20, 21]. The immense potential of binary GNN inference on hardware has not yet been harvested.

Quantizing tensors into bits and representing and manipulating them efficiently on word-based architecture involves lots of intricacies. It is even more so for GNNs, for several reasons. First, a GNN layer typically consists of interleaving dense and sparse operators. It is not straightforward to reconcile the inconsistency between dense and sparse bit-width layouts while minimizing the inference latency and facilitating the attainment of desirable accuracy-speed tradeoffs. Second, in binary GNNs, the meaning of bits in activations/weights (1/0 means +/-) and graphs (1/0 means connectivity) differ. To fit such unique properties, integer intrinsics should be carefully orchestrated to maximize bit-level and thread-level parallelism. Third, to fully harness the significant memory reduction brought by bit storage, it is important to synergize the careful use of registers and memory hierarchy with the massive parallelism on accelerators.

This work provides the first known systematic exploration to unlock the performance potential of binary GNNs. The target hardware it focuses on is Graphics Processing Units (GPUs), the most commonly used device for GNNs and binary GNNs. This work makes four-fold contributions:

(1) Materializing binary GNNs with a series of bit-level-optimized abstraction. To fulfill a binary GNN model, various compositions of bit-level BLAS kernels with different choices of precision, elimination of rebinarization, or fusion decisions can exist. We propose the first two-level Binary GNN abstraction, which hides the complexities from users, offers flexible support of various scenarios and enables easy drop-in replacements for converting a GNN into a binary GNN.

(2) Representation of bit tensors. Binary GNN includes binarized activations, weights, and adjacency matrices. Unlike activations and weights, adjacency matrices are typically sparse, the representation of which is subject to a granularity dilemma. We propose a *fine-representing dynamic-coarsening* (FRDC) scheme to simultaneously minimize graph storage cost and maximize kernel efficiency on a GPU. Additionally, we propose several solutions to reconcile the 1/0 and +/- inconsistency between binary graphs and activations.

(3) Materialization of the BitGNN abstractions. We develop the BitGNN abstractions into an efficient library through careful bit manipulations via binary intrinsics and memory and parallelism optimizations. We devise and materialize the abstractions for different precision needs with bit-manipulation intrinsics. We propose a series of techniques with dedicated treatment on workload decomposition, bit-tensor load/store with registers and on-chip memory usage, and intra-warp and inter-warp synchronizations. The implementation builds on insights in conventional binary DNNs but joins significant new features, including the first set of binary sparse matrix multiplication (BSpMM) kernels.

(4) Evaluation of BitGNN. We integrate all the techniques into a full solution, namely BitGNN, in the form of a collection of a library and tuning utilities. Compared to the state-of-the-art binary GNN [18] and full-precision GNN [22] implementations, BitGNN gives up to 26X, 22X, and 19X latency reduction on GCN, GraphSAGE and GraphSAINT models. Meanwhile, BitGNN makes GNNs possible to efficiently process several graphs that are too large to process by prior solutions.

2 BACKGROUND

2.1 Graph Neural Networks

There are typically two types of operations in a GNN: *aggregate* and *apply*. The *aggregate* phase collects the information from the input graph's geometric structure. The *apply* phase performs linear or non-linear operations as in typical Neural Networks. A GNN can be formulated as follows:

$$\mathbf{X}_i^{(l+1)} = \gamma_\theta \left(\mathbf{X}_i^{(l)}, \Psi_{j \in \mathcal{N}(i)} \phi_\theta \left(\mathbf{X}_i^{(l)}, \mathbf{X}_j^{(l)}, \mathbf{E}_{i,j} \right) \right)$$

For node classification tasks, the node representation is the activation in each GNN layer. The representation of node i at layer l is denoted as $\mathbf{X}_i^{(l)}$. $\mathcal{N}(i)$ represents the set of neighbors of node i . In an *aggregate* phase, Ψ denotes a permutation-invariant function that performs message aggregation. The commonly used functions include sum, mean, and max. Before the aggregation, ϕ_θ denotes any user-defined operators applied to the following: \mathbf{X}_i (the representation of node i), \mathbf{X}_j (the representation of node j , the neighbors of node i), or $\mathbf{E}_{i,j}$ (the representation of edge (i, j)). After the aggregation, γ_θ denotes the operations of the *apply* phase. Most GNNs have neural operations (e.g., MLP and ReLU) in this phase. We briefly explain several popular GNNs.

GCNConv Graph Convolutional Networks (GCNs) [7] introduces a semi-supervised learning algorithm that can learn the graph structure directly. A forward layer of GCNConv can be defined as follows:

$$\mathbf{X}^{(l+1)} = \sigma(\tilde{\mathbf{A}}\mathbf{X}^{(l)}\mathbf{W}^{(l)}),$$

where the normalized adjacency matrix $\tilde{\mathbf{A}} = \hat{\mathbf{D}}^{-\frac{1}{2}}\hat{\mathbf{A}}\hat{\mathbf{D}}^{-\frac{1}{2}}$. The $\hat{\mathbf{A}} = \mathbf{A} + \mathbf{I}$ is the adjacency matrix plus self-adjacency, and $\hat{\mathbf{D}}_{ii} = \sum_{j=0} \hat{A}_{ij}$ is its diagonal out-degree matrix. $\mathbf{X}^{(l)} \in \mathbb{R}^{N \times d}$ denotes the node feature embedding in the l -th layer, and $\mathbf{W}^{(l)}$ is the learnable parameters or weights, and σ represents a non-linear activation function (e.g., ReLU). Bi-GCN [18] is composed of two such GCNConv layers.

SAGEConv SAGEConv [23] enhances the graph convolution layer with a mean aggregator as it is a linear approximation of a localized spectral convolution [7]. It also extends the layer with a skip connection to emulate the concatenation of the prior layer's node representation in the convolutional aggregator. A SAGEConv layer is defined as follows:

$$\mathbf{X}_i^{(l+1)} = \mathbf{X}_i^{(l)}\mathbf{W}_1^{(l)} + \text{mean}_{j \in \mathcal{N}(i)} \mathbf{X}_j^{(l)} \cdot \mathbf{W}_2^{(l)}$$

GraphConv GraphConv [24] is similar to SAGEConv except that it uses a normal sum aggregator:

$$\mathbf{X}_i^{(l+1)} = \mathbf{X}_i^{(l)}\mathbf{W}_1^{(l)} + \sum_{j \in \mathcal{N}(i)} \mathbf{X}_j^{(l)}\mathbf{W}_2^{(l)}$$

To allow learning on large graphs, GraphSAGE [23] proposes a neighbor sampling approach to deal with the neighbor explosion problem on large graph training. Bi-GraphSAGE [18] is composed of two such SAGEConv layers. GraphSAINT [25, 26] introduces a graph sampling-based inductive learning approach. The Bi-GraphSAINT [18] model referred to in this paper comprises two GraphConv layers and a fully-connected layer.

2.2 Binary Neural Networks

A bit-dot-product between two 0/1 bit-vectors can be computed as follows:

$$c = \text{popc}(a_{(b)} \& b_{(b)}),$$

where $\&$ denotes logic AND operation and $\text{popc}()$ is the population count function that counts the number of 1 bits.

In binary neural networks (BNNs) [13–16], the binarization function is often defined as follows:

$$x_{(b)} = \text{sign}(x) \begin{cases} 1, & \text{if } x \geq 0 \\ -1, & \text{otherwise} \end{cases}$$

The bit-dot-product operation of +1/-1 bit-vectors can be computed through:

$$c = n - 2 \times \text{popc}(a_{(b)} \oplus b_{(b)}) = 2 \times \text{popc}(a_{(b)} \odot b_{(b)}) - n$$

where \oplus is exclusive-OR (XOR), \odot is exclusive-NOR (XNOR), and n is the *bit-width* of $a_{(b)}$ and $b_{(b)}$.

2.3 Bit-ops Intrinsics

Other than commonly-seen logical AND ($\&$), OR(\mid), XOR (\wedge), negation (\neg), bit left-shifting (\ll) and right-shifting (\gg), GPUs are equipped with several integer intrinsics that can be used for efficient bit operations. `__popc()` and `__popcl()` allow fast bit-accumulation of a single 32-bit or 64-bit unsigned integer. `__shfl_sync()` is for register data exchange between threads in a warp [27]. By indicating the thread lane to exchange, the intrinsic will receive register data from the designated thread lane. `__ballot_sync()` is a warp-voting intrinsic used for register data exchange between threads in a warp. Assuming all threads in a warp are active, it will return a bit-masked 32-bit unsigned integer showing the boolean evaluation result of the predicate-argument in each thread. It is the same as a clockwise transpose of a bit-column into a bit-row and can be useful for fast binarizing the full-precision values with a warp of threads. `__brev()` and `__brevll()` reverse the bit-order of a 32-bit and a 64-bit unsigned integer, respectively. When paired with `__ballot_sync()`, they can be helpful in rotating a bit-column 90° anti-clockwise into a bit-row [28]. Our implementation of efficient binary GNN is based on those intrinsics. As similar intrinsics can be found in other vendors' GPUs [29], our BitGNN is portable to other GPU platforms.

3 BITGNN

Our design of BitGNN aims to achieve (i) efficiency: a GNN using BitGNN should enjoy a significantly higher speed; (ii) accuracy: a binary GNN that uses BitGNN should be able to get the same accuracy as the binary GNNs by prior approaches do; (iii) ease to use: with BitGNN, users should be able to convert a GNN into a binary GNN easily; (iv) flexible to tune: Different GNNs may require a different accuracy-speed objective; with BitGNN, users should be able to tune the tradeoff easily.

This section presents our design. The design of BitGNN consists of a set of novel abstractions, representations, algorithms, and optimizations. The final materialization is a library and utilities that users can use to build and tune their efficient binary GNNs easily.

Two key components of a GNN are operations and tensors. Correspondingly, our creation of BitGNN centers around three key

research questions: (R1) What should be the abstractions of common binary GNN operations? (R2) How should binary tensors be represented? (R3) How to assemble them into efficient ready-to-use libraries?

3.1 R1: What should be the abstractions of common binary GNN operations?

GNNs have many kinds, and their binarized forms may consist of even more complexities and variations, depending on which part of the GNN is binarized for good accuracy-speed tradeoffs. For BitGNN to be easily applicable to various GNNs, it is hence important to abstract the common binary GNN operations into some building blocks. The result of such an abstraction must cover the most important operations of various binary GNNs, and at the same time, support their different needs in binarization. To the best of our knowledge, no prior work has studied systematic abstractions of binary GNN operations.

3.1.1 Complexities. To better understand the complexities in designing binary GNN operations, this part provides a deeper look at the binarization process. We explain it by taking GCN as an example.

The top graph in Figure 1 illustrates the original GCN [7]. A forward pass of GCN involves two GCNConv layers followed by a softmax. Each GCNConv layer starts with a matrix-matrix multiplication (MM), where the input activation is multiplied by the weight matrix. The result at each graph node is then aggregated with its neighbor nodes' results, which is carried out by multiplication with the adjacency matrix of the graph. Because the adjacency matrix is typically sparse, the second matrix multiplication can use sparse matrix multiplication (SpMM).

Below the original GCN in Figure 1 are three variations of the binarized form of the GCN. The first, Bi-GCN-1, is the form described in a previous work [18]. It replaces the first MM with binary matrix multiplication (BMM). To do that, it binarizes the weight matrix offline. It inserts into the GCN computation graph three extra operations, a batch normalization (BN), and a tensor binarization (BIN) before BMM. A scaling operation (SCL) after BMM to recover the scale of the results. It replaces the second MM with BMM and inserts a BIN before BMM and an SCL operation after BMM.

This binarized form considers only the binarization of the two MM operations. Other operations in the original GCN could be binarized, possibly at different degrees. For instance, Bi-GCN-2 in Figure 1 shows a variant where the two SpMM operations are “half” binarized—that is, the adjacency matrices are binarized, but the activation maps are not. On the other hand, Bi-GCN-3 in Figure 1 shows a case where the two SpMM operations are fully binarized, with more auxiliary operations added. All three variants could have their merits: As binarization applies more, there are potentially more speedups and more risks in accuracy loss. It is easy to see that besides these three variants, there can be many other variants, each corresponding to the combination of the operations binarized to a certain degree.

Even more, complexities are there if the GNN contains more operations, as exemplified by the original architecture of SAGE and SAINT on the top of Figure 2. Our studies of many common GNNs and their binarized forms lead us to the following observations:

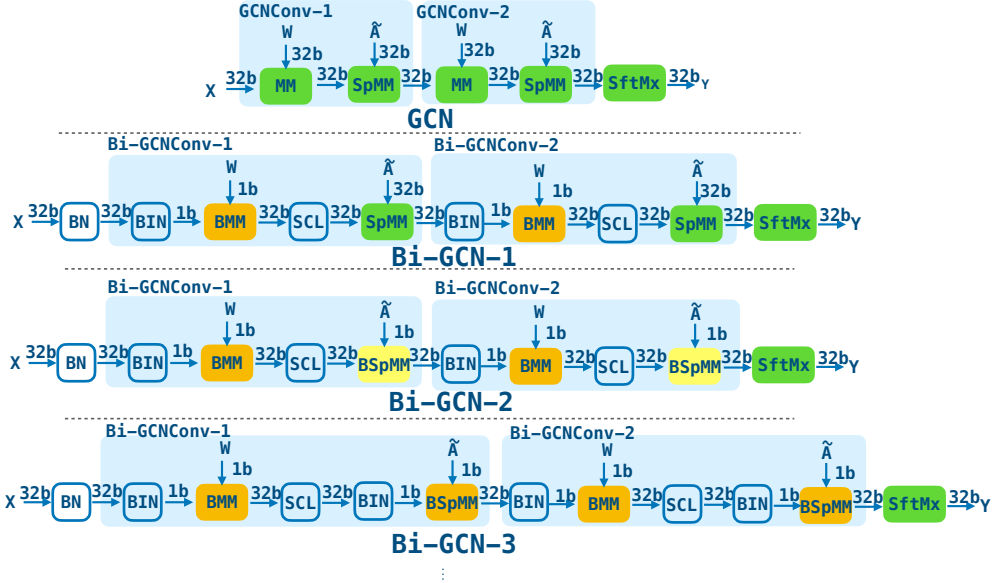


Figure 1: Illustration of the original full-precision GCN [7], and several variants of binary GCN.

(i) One GNN may have many possible binarized forms, each containing many extra operations.

(ii) A simple one-on-one mapping is insufficient. After different binarizations, one operation in the original GNN may be replaced with different sequences of operations. Creating one abstraction for the binarized form of one original operation is hence insufficient.

(iii) There are, however, a set of operations that compose the core operations of binary GNNs. The variants in Figure 1, for instance, are all composed of BN, BIN, BMM, SCL, SpMM, and softmax, despite the differences in their specific connections and architectures. This also appears on other GNNs because most GNNs have MM and SpMM as their core operations.

3.1.2 Two-level BitGNN Abstraction.

Based on the observations, we design a two-level BitGNN abstraction. We adhere to the following principles in our design.

(1) Coverage: The abstraction should cover the most time-consuming core parts of common GNNs.

(2) Flexibility: The abstraction should support the need for different accuracy-speed tradeoffs.

(3) Efficiency: The abstraction should be conscious of the implications to computing efficiency.

(4) Easy to apply: The abstraction should allow easy adoption in GNN development such that a GNN can be easily revised into a binary GNN. Further, it should support easy tuning of the binarization process for meeting the different accuracy-speed objectives.

The bottom in Figure 2 shows the core components of the abstraction. The low-level functions offer the primary building blocks, while the high-level functions provide options for drop-in replacement of the components in GNNs for binarization. The former gives flexibility, while the latter gives ease of use.

Low-level functions. The low-level functions are in three groups. The first group is about the binarization of matrix multiplication (MM). One of the performance bottlenecks in prior binary GNN materialization is the re-binarization of the activation tensors in

each layer. Our design of the functions takes that into consideration. Specifically, we include seven variants of BMM, each corresponding to a different combination of the precisions of the input activation, the weight matrix, and the output, as shown at the bottom of Figure 2. The precisions determine what auxiliary operands are needed (e.g., Full-precision inputs would need to go through BIN to be binarized before participating in the multiplication). In our design, these operands are included inside the BMM functions to avoid the invocation overhead and the need for complex kernel fusions.

One of our insights is that when BIN immediately follows SCL, the SCL becomes meaningless and can be removed. The reason is that the scaling factor is positive², so the element-wise multiplication of the scaling factor will not affect the binarization result.

The second group is about SpMM. They are typically used for the multiplications that involve adjacency matrices [30]. Our design of the binarized forms includes eight variants, as shown at the bottom of Figure 2. The reasons for those variants include the accuracy-speed tradeoff, as in the BMM case, and the special property of adjacency matrices. In GNN workloads, the connections between two nodes may or may not carry weights. In the former case, only 0/1 values are in the adjacency matrix representing node connectivity. In the latter case, BSpMM can still be applied: There is a standard approach to binarize an adjacency matrix through factorization. There will be a multiplication with a full-precision factorization vector following the matrix multiplication.

The third group concerns some auxiliary operations (e.g., the add operations for self-connectivity and the concatenation operations). As the binary operations may output results of different precisions, this group consists of several variants. Unlike the other operations, for these two operations, mixed precisions of their operands are not meaningful in practice. Our design hence excludes those variants.

²In Bi-GCN [18], for instance, the scaling factors are the row-wise and column-wise L1 normalization values.

Notation: for convenience, the following discussion uses a **three-letter suffix** to distinguish the variants of an operator: For instance, BSpMM.FBB represents BSpMM that takes in a full-precision (F) matrix (1st operand) and a binary (B) matrix (2nd operand) as inputs and produces a binary (B) matrix.

High-level functions. The low-level functions cover the most essential operations in binary GNNs and provide flexibility in meeting various needs. To further ease the adoption, we have also designed a set of high-level functions to allow easy drop-in replacement of key time-consuming operations in a GNN for binarization. Our studies show that despite the large variety of GNNs, their most time-consuming core operations are two, matrix multiplications (MM) and sparse matrix multiplications (SpMM). The high-level functions hence center around those operations and their combinations.

Those functions are in two groups, each combining multiple low-level functions. The first group is for a typical case where BSpMM immediately follows BMM, as exemplified by GCN in Figure 1. The variants come from the activation tensor between the BMM and SpMM. It can either be in the binarized form or full-precision form. Consequently, we have BMM.FBB+BSpMM.BBB or BMM.FBF+BSpMM.FBB for the first GCNConv layer. Similarly, we can have BMM.BBF+BSpMM.FBF or BMM.BBB+BSpMM.BBF for the second GCNConv layer. The second group is for another common case where some auxiliary operations follow MM, as exemplified by the architecture of SAGE in Figure 1. The auxiliary operator comes from self-connectivity, for which we can use either ADD.BBF or ADD.FFF to merge the activation output at the end of the first SAGEConv layer.

The top of Figure 2 illustrates how the three GNNs can be easily converted into binary GNNs by simply replacing the common patterns of operation sequences with the corresponding high-level functions. The low-level functions with small latency, like ADD, are fused to BMMs or SpMMs, while high-level functions are optimized through inter-layer fusions between BMMs and BSpMMs using cooperative kernel launch to improve thread block synchronization. Moreover, with the high-level functions, it is easy to tune the binary GNN for accuracy-speed tradeoffs. For the GCN.bin in Figure 2, the user may replace its two MM-SPMMs with other options in the high-level function set. As long as a predecessor block's output precision matches its successor's input precision, the correctness of types is guaranteed, while the accuracy and speed may vary.

To summarize, the design of BitGNN's high-level and low-level abstractions provides good coverage of the possible decision space for binary GNN architecture exploitation. Specifically, at the low-level, the design covers the various needs of precisions of the core operations and minimizes invocation overhead. At the high-level, the design eliminates unnecessary rebinarization, offers to tune flexibility for accuracy-speed tradeoffs, and enables simple drop-in replacement for converting GNNs into binary GNNs.

3.2 R2: How to represent binarized tensors?

Representation of binarized tensors determines how efficiently a binarized GNN consumes memory and how fast it can access the data it needs. Existing binary GNN implementations [13–16] do not really place the activation or weight tensors in bits, nor do they consider storing the graph in bits.

Some work in conventional DNN has studied the representation of binary tensors and proposed several representations [28, 31]. Two special complexities in GNN, however, call for innovative solutions. We next focus our discussion on each of the complexities and our solutions.

3.2.1 Granularity Dilemma. The first complexity is about the granularity of representations.

Dilemma. There are many representations proposed for sparse matrices. One of them that shows an especially good fit for adjacency matrices is block-based representation [30], where the matrix is viewed as a composition of many k -by- k blocks; each block's content is stored in a dense format, but the block-level representation uses a sparse format (e.g., CSR) with all-zero blocks being ignored.

This representation, however, faces a dilemma in block size. The smaller the block is, the fewer zeros will be included in the representation, but at the same time, it leads to more reduction operations among blocks; a smaller block is also less friendly to the massive parallelism of the GPU.

Solution. To address the granularity dilemma, we propose *fine-representing dynamic-coarsening (FRDC)*, a scheme that uses the fine-grained representation to achieve high space efficiency and on-chip coarsening to attain high time efficiency. Specifically, FRDC uses 4×4 as the block size for representation. The reason for using 4×4 bit-blocks is to use fine-grained representation to store matrices but use online stitched coarse-grained representation for computations. The former saves the storage and memory space, while the latter better exploits bit-level parallelism. If 4×8 or 8×4 blocks are used, the memory usage doubles; if smaller tiles are used, the dynamic stitching overhead increases. Our empirical results show that 4×4 is generally a sweet spot.

During computations, the 4×4 bit-blocks (containing 16-bits) are moved from GPU DRAM to shared memory/registers, and our BitGNN kernel on-the-fly assembles the 4×4 bit-blocks into 32-bit aligned words on shared memory and uses word-level bit manipulation intrinsics (see Section 2.3) to process them efficiently. Such a scheme maintains the space benefits of the fine-grained representations while simultaneously delivering maximal parallelism.

3.2.2 Inconsistent Value Ranges. The second special complexity comes from the different ranges of the values of tensors after binarization.

A common place where the complexity arises is the discrepancy between adjacency matrices and activation maps. The adjacency matrix uses 1/0 to indicate edge connectivity, so the basic operation is 0/1 dot-product. However, the binary neural network activation uses the +1/-1 dot product instead. The question is how to conduct multiplications between them efficiently. Previous studies have not addressed the problem.

In this work, we explore three methods to reconcile the incompatibility. In explaining the methods, we use a to denote a 0/1-based bit-vector of the adjacency matrix and b_{org} a +1/-1-based bit-vector from the activation matrix. In memory, both a and b_{org} are represented in 0/1 bits; for the sake of explanation, we introduce b to denote the 0/1 in-memory representation of b_{org} , where 1 is for +1 and 0 for -1. We now explain the three methods to compute the dot product between a and b_{org} .

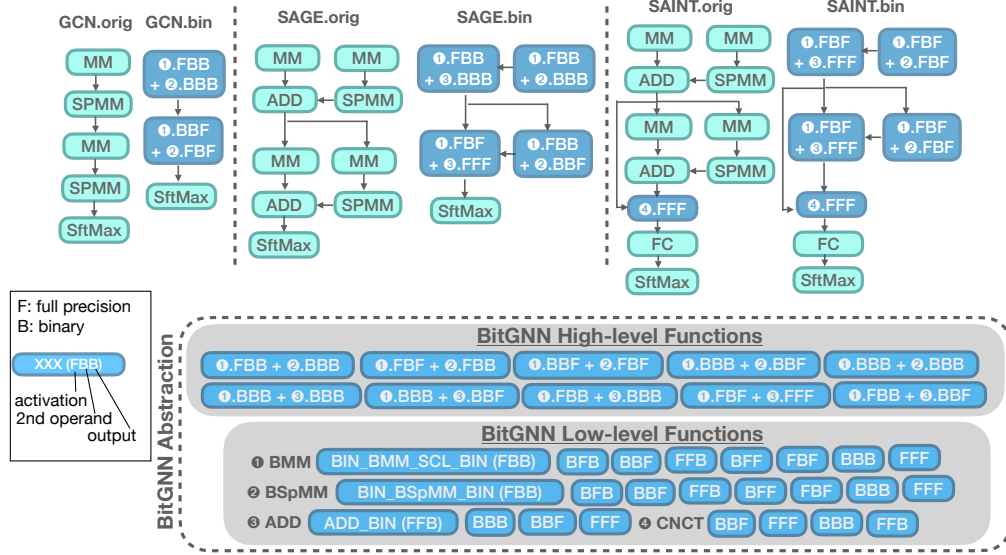


Figure 2: Core components of the two-level BitGNN abstraction (bottom) and its usage examples (top). At the low-level, BitGNN supports the core kernels in bit-ops, including ① BMM (Bit-MatMul) ② BSpMM (Bit-Sparse-Dense-MatMul) ③ ④ Auxiliary Ops. At the high-level, BitGNN provides fused operators for binary or full-precision operand input/output. In the usage examples, "orig" and "bin" suffixes represent the original and binary forms of the GNNs, respectively.

(1) If-else evaluation on a 's nonzeros: This method checks each bit of a . If the value is 1, we accumulate the corresponding bit in b ($1 \rightarrow 1, 0 \rightarrow -1$) to the temporary sum; otherwise, we bypass the bit value in b .

(2) $popc(a \& b) - popc(a \& \neg b)$: $popc(a \& b)$ accumulates the total number of 1s of $a \times b$. $popc(a \& \neg b)$ ($\neg b$ is the complement of b) gives the total number of -1 in b_{org} . Subtracting the two results, we can obtain the dot product of a and b_{org} .

(3) $2 \times popc(a \& b) - popc(a)$: The transformation from the $+1/-1$ to $1/0$ is to add 1 and then divide 2 (i.e., right shift), that is, $b = (b_{org} + 1)/2$. Hence, $b_{org} = 2 \times b - 1$. As $popc(a \& b)$ is the bit-dot-product of a and b , the dot-product of a and b_{org} can be calculated as $2 \times popc(a \& b) - popc(a)$.

When activation values are in bits, Solution-2 and Solution-3 work much more efficiently than Solution-1; in other cases, Solution-1 can enable the computation between the binary adjacency matrix and the full-precision activation. Section 3.4 gives more discussions on the selection.

3.3 R3: How to realize the potential in coding?

The third research question is about effectively materializing the BitGNN abstractions to best leverage the binary representations of tensors for efficiency.

Previous work on binary GNN [18–20] falls short on this aspect. They only simulate the binarization with `sign()` function and FP32 multiplication. They do not actually treat a value as a bit in the implemented operations.

Our solution carefully explores bit manipulation intrinsics offered by modern GPUs to unlock the performance potential fully. In BitGNN, the core operations are BMM and BSpMM, as shown

in Figure 2. Both have some variants. BMM has been studied before [28, 31]; the ones in BitGNN built on the prior work while considering the various precisions and the fusions of the auxiliary operations. BSpMM, however, has not been studied before. Our following discussion hence focuses on BSpMM.

3.3.1 Design Principles. The BSpMM kernels with our FRDC-based tensors are designed with the following principles: (1) *Warp-based workload partition*. We map each workload unit of a node into one or more warps and fully utilize the fast intra-warp communication [32] on GPUs. (2) *Maximizing bit-level parallelism*. This addresses the granularity dilemma mentioned earlier and maximizes the edge traversal throughput (number of traversed edges per second (TEPS)). It is required that the small bit-blocks in sparse graphs are ultimately manipulated in a word-aligned fashion. (3) *Maximizing bit-tensor load & store efficiency*: SpMM is usually memory-bound [33, 34]. Careful use of memory hierarchy for bit-tensor manipulations is hence essential.

3.3.2 Implementations. Following the three principles, we materialize the BitGNN abstractions with the FRDC scheme and bit-manipulation intrinsics. We explain the implementation of BSpMM.BBB in detail as an example.

BSpMM.BBB Algorithm 1 presents the BSpMM.BBB kernel implementation using FRDC technique. The input binary adjacency matrix is represented using RowPtr, Collnd, and BitTiles (BitBlock)³. Since the algorithm is parallelized through the tile (block) row dimension, we present tile (block) row r 's workload here. It is processed by a warp of 32 threads.

In Line 1, we divide each tile-row's total number of tiles (NT) into several tilesets. The size of a tileset (TS) is defined as the

³We use the terms "tile" and "block" interchangeably in the paragraphs.

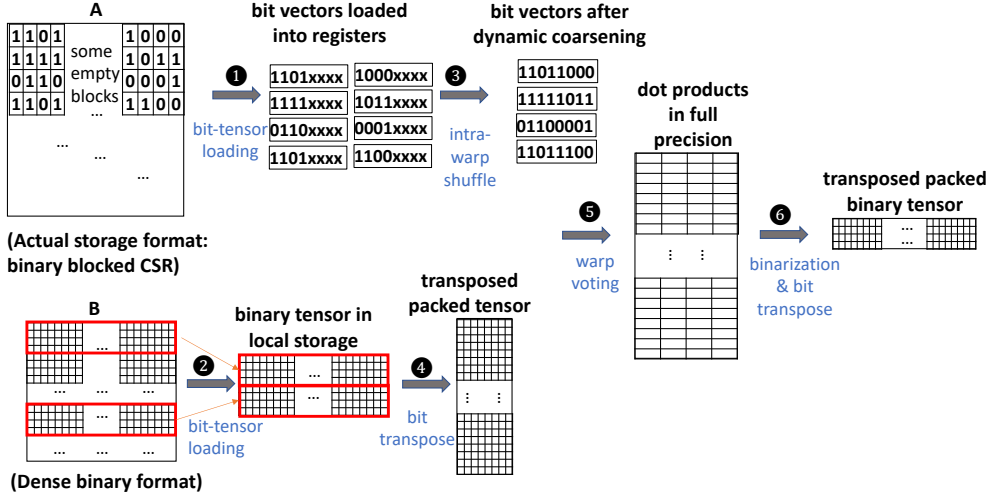


Figure 3: Illustration of the procedure of BSpMM.BBB using FDRC (Fine-Representing Dynamic-Coarsening).

Algorithm 1: BSpMM.BBB

Input: AdjMat: RowPtr, ColInd, BitTiles, Tile-row ID r ;
InActMat $_{(b)}$;
Output: OutActMat $_{(b)}$

- 1 $NT \leftarrow \text{RowPtr}[r+1]-\text{RowPtr}[r]$; $TS \leftarrow \frac{\text{SIMD_unit}}{\text{tile_dim}}$
- 2 **for** each tile set t_s where $s = 1$ to $\lceil \frac{NT}{TS} \rceil$ **do**
- 3 **register** $A \leftarrow \text{BitTiles}[s]$ for $s = 0$ to $TS-1$
- 4 **register** $B \leftarrow \text{InActMat}_{(b)}[k]$ for $k = \text{ColInd}[s] \times \text{tileDim} + \{0, 1, 2, \dots, \text{tileDim}-1\}$ and $s = 0$ to $TS-1$
- 5 **register** $a \leftarrow a \mid \text{shfl}(A, s \times \text{tile_dim} + \text{laneid}) \ll (4 \times (TS-1-s))$ for $s = 0$ to $TS-1$ // do bit-concatenate
- 6 **shared memory** $b[warpid \times \lceil \frac{32}{W} \rceil + k] \leftarrow \text{brev}(\text{ballot}((B \gg (31-k)) \& 0x1))$ for $k = 0$ to $\text{SIMD_unit}-1$ // do bit-transpose
- 7 **register** $c[n] \leftarrow \text{popc}(\text{shfl}(a, n) \& b[warpid \times \lceil \frac{32}{W} \rceil + \text{laneid}] - \text{popc}(\text{shfl}(a, n) \& \neg b[warpid \times \lceil \frac{32}{W} \rceil + \text{laneid}]))$ for $n = 0$ to $\text{tileDim}-1$ // compute bit-dot-product
- 8 **register** $rs[n] \leftarrow \text{brev}(\text{ballot}(c[n] \geq 0))$ for $n = 0$ to $\text{tileDim}-1$
- 9 **OutActMat** $_{(b)}[r \times \text{tileDim} + n] \leftarrow rs[n]$ for $n = 0$ to $\text{tileDim}-1$

number of bit-row required to concatenate into a *SIMD unit*, which is equal to $\frac{\text{SIMD_unit}}{\text{tile_dimension}}$. For example, when the adjacency matrix is stored in the block-4 \times 4 format with 4 \times 4 non-empty tiles, a non-empty tile contains four nibbles (4-bit). When we use 32 as a *SIMD unit*, the tileset size (TS) equals 8. Consequently, in Line 2, the kernel will process 8 bit-tiles in each iteration. A tileset (TS) is the processing unit of an iteration. Therefore, the workload of each tile-row requires $\lceil \frac{NT}{TS} \rceil$ of iterations to accomplish.

In this case, the adjacency matrix (A in Figure 3) and the input activation (B in Figure 3) are both binary, and the output should be binary as well. As illustrated in Figure 3, the algorithm consists of the following steps:

Step ① & ② Warp-based workload partitioning and loading. Each warp of 32 threads is mapped to the computation of a row of 4 \times 4 bit-tiles (4 nodes when representing the graph in bits). Within each warp, the row of bit-tiles is further partitioned into multiple tile

groups of 8 bit-blocks. For example, if there are ten bit-tiles, there will be a total of two tile groups. The first tile group holds the 0th-7th tiles of that 4 \times 4 tile row; the second tile group holds the 8th and 9th tiles, with the remaining 8 slots padded with zero. Next, each iteration processes a tile group as follows: the 32 threads cooperatively load the 32 uchar⁴ of 8 bit-tiles of A (sparse bit matrix) from global memory into registers, and then the 32 threads load the 8 segments of B corresponding to the loaded tiles of A from global memory into shared memory, forming a consecutive layout, with each word used as a 32-bit vector.

Step ③ On-the-fly assembly via bit-concatenation. This step conducts dynamic coarsening, making the bit-tiles of A 32-bit aligned. Each of the 0th-3rd threads leverages the intra-warp communication intrinsic (i.e., `shfl_sync()`) and bit shifting to fast concatenate neighbors of each node (in the form of bit-vectors) into a 32-bit unsigned bit-vector (only 8-bit shown in our illustration in Figure 3).

Step ④ Bit-transpose for column-wise coalesced access. This step transposes the column-major packing of B into row-major. In this way, when computing the bit-dot-product with A, the bits can be fetched as bit-columns, and the bit-level parallelism can be fully employed. The transpose is through bit shifting and masking on the bit-vector of B. The values are then evaluated and gathered through the intra-warp voting intrinsic (i.e., `ballot_sync()`). Next, they are transposed by the `brev()` intrinsic.

Step ⑤ Trinary-valued bit-dot-product. This step computes the bit-dot-product between 0/1 bit-vectors of A and +1/-1 bit-vectors of B. (“Trinary” for 0/1/-1.) A loop of 4 iterations (each for one node) works on a 32-bit bit-vector from A. Each of the 32 threads is responsible for 1/32 of the bit-dot-product calculations. The products are stored in the registers as full-precision values.

Step ⑥ Bit-tensor store. This step packs the temporary full-precision products into the bit format. It is through element-wise evaluation of whether the product is greater than or equal to 0 (i.e.,

⁴We store 4-bit unit as an uchar (1 byte) in our original implementation. Storing them in a smaller representation (i.e., int4) is also possible in newer GPU architectures.

the binarization process of binary activation tensor). The 32 threads of a warp can evaluate the full-precision values with intra-warp voting intrinsic (i.e., `ballot_sync()`). Then, it performs an anti-clockwise transpose of the result by the `brev()` intrinsic to complete the bit-vector packing. The result produces 32-bit unsigned bit-vectors of the activation map.

Other variants The implementations of other variants of BSpMM follow a similar approach, with bit-level intrinsics used for most of the computations and some differences for handling the different precisions. BSpMM.FBB, for instance, loads the activation tensor differently. In step ② (bit-tensor load), it requires 4 warps to cooperatively load all the full-precision values, with each thread in a warp responsible for loading one of the dimensions of the feature vectors of 32 neighbor nodes. Subsequently, step ④ (Bit-transpose for column-wise coalesce access) is not needed. More details are presented in our supplement material [35].

3.4 Tuning Utilities and Other Implementation Details

To launch the end-to-end model that contains multiple kernels, we use `cudaLaunchCooperativeKernel()` to allow global synchronization between a certain set of thread blocks [36]. We calculate the maximum number of blocks that fit each SM with `cudaOccupancyMaxActiveBlocksPerMultiprocessor()` and use 1024 threads per thread block. This allows the maximum number of warps to execute on each SM.

In addition to the library, BitGNN also contains a set of utilities that facilitate the tuning of Binary GNNs. As the previous sections have shown, BitGNN offers a set of variants to meet the different needs of precisions in the inputs, weights, and outputs in different GNNs. With BitGNN’s tuning utilities, an auto-tuning run can replace the invocations of the BitGNN functions in a GNN with other variants and observe the performance; the correctness of types is guaranteed by ensuring the precision of the output of a predecessor is the same as that of the input of its successor operation. Similarly, the tuner can easily select the best solutions to reconcile the inconsistency of binary value ranges as mentioned in Section 3.2.2. It is possible to build up predictors to predict the best variant to use for a given GNN and graph. Similar predictors in other contexts (e.g., predictors of sparse matrix storage formats [37]) have been well studied.

4 EVALUATION

This section reports the performance of BitGNN. We focus on the following questions: (i) How much speedup can it bring to GNN inferences? (ii) How much memory space can it save? (iii) What are the accuracy-speed tradeoffs when using BitGNN?

4.1 Methodology

GPU Environment: We evaluate the performance of BitGNN on three NVIDIA GPUs of different architecture generations: GTX 1080 (Pascal), Titan V (Volta), and RTX 3060 Ti (Ampere). Their features are summarized in Table 1. The CUDA version is 11.0. For all experiments, we use the average values of 10 repeated executions.

Datasets: Table 2 shows the graphs used for the evaluation. These graphs are commonly used for existing GNN research [23, 25, 26, 38–41] and are also the graphs used in prior binary GNN work Bi-GCN [18], making direct comparisons possible.

Versions to compare: We compare our BitGNN versions (of different revisions) with Bi-GCN [18]. As the representative of the state-of-the-art binary GNNs—which all focus on binarization algorithms rather than optimized executions, Bi-GCN uses the full-precision representation of values even though it binarizes the operations in GNNs. Meanwhile, to provide a reference point, we report the performance and accuracy of the original GNNs without binarization. Both the original and Bi-GCN versions are in PyG [22].

GNNs: We use four GNNs in our experiments: transductive-GCN [7], inductive-GCN [23], GraphSAGE [23], and GraphSAINT [25, 26]. We choose these GNNs because they are the most popular GNNs, and are the GNNs used in the prior binary GNN study [18] that we compare with.

4.2 Results and Analysis

Tables 3, 4, and 5 report the speed (at inference time), accuracy, and space usage of the baselines and the versions of our BitGNN.

Before diving into the results, it is worth mentioning that GNN learning is of two kinds: transductive and inductive learning. In transductive learning, the entire data graph is observed in the learning process, with some nodes labeled and others not. The GNN algorithm tries to iteratively refine the labels of those unlabeled nodes by learning from the entire graph structure and those labeled nodes. In inductive learning, the GNN algorithm learns from some sampled graphs and then tries to predict the labels of the nodes on other sampled graphs.

Among the four GNNs used in prior research [7, 23, 25, 26], *transductive-GCN* is for transductive learning, and the other three GNNs are for inductive learning. The prior work applies *transductive-GCN* to only small datasets (Cora, PubMed, CiteSeer) because large graphs are difficult to be loaded and processed in memory as an entirety as required by transductive GNNs. For the large datasets (Flickr and Reddit), the prior work applies the three inductive GNNs. To allow head-to-head comparisons, our experiments follow the same practice.

The proposed flexible programming abstraction (Section 3.1.2) can easily facilitate the user’s binary network development. With it, we tune the various binarization precisions and identify some model variants that perform relatively well: *full-precision aggregation* (the same as in Bi-GCN [18]) and *binary aggregation* (Use MM.FBB + BSpMM.BBB for the first layer and MM.BBF + BSpMM.FBF for the second layer). They are represented as *Ours (full)* and *Ours (bin)* in the result tables.

Transductive case: From Table 3, we have the following observations. (i) Both versions of BitGNN can keep most of the accuracy. The largest loss of the average accuracy is 0.2%, 0.9%, and 2.2% on the three datasets, respectively. The largest accuracy loss (2.2%) happens on *CiteSeer*, where the normalization of edge weights has a more significant impact. (ii) Both versions can save memory usage significantly, 7–19X by *Ours (full)* and 18–28X by *Ours (bin)*. (iii) Both versions consistently show significant speedups across GPU models. The speedups are 1.2–5X by *Ours (full)* and 4–7X by *Ours*

Table 1: GPUs used for evaluation. Arch refers to GPU architecture generation. CC refers to compute capability. SMs refer to the number of streaming multiprocessors in the GPU. Thrds refer to threads. Shared refers to share memory size. Reg refers to number of registers. Note, "/Block" and "/Thrd" imply the maximum resources per thread block and per thread, respectively.

GPU	Arch	CC	SMs	DRAM	Memory Bandwidth	L1 Cache Size/SM	L2 Cache Size	Warps /SM	Blocks /SM	Thrds /SM	Shared /SM	Shared /Block	Reg /SM	Reg /Block	Reg /Thrd
GTX 1080	Pascal	6.0	20	8GB	320GB/s	48KB	4096KB	64	32	2048	64KB	48KB	64K	64K	255
TITAN V	Volta	7.0	80	12GB	653GB/s	96KB	4608KB	64	32	2048	96KB	96KB	64K	64K	255
RTX 3060 Ti	Ampere	8.0	38	8GB	448GB/s	128KB	4096KB	64	32	2048	164KB	164KB	64K	64K	255

Table 2: Graph datasets used for evaluation.

Dataset	#Nodes	#Edges	#Features	#Classes
Cora	2,708	13,264	1,433	7
Pubmed	19,717	108,356	500	3
Citeseer	3,327	12,431	3,703	6
Flickr	89,250	899,756	500	7
Reddit	232,965	114,615,892	602	41

Table 3: Evaluation results of transductive GCNs. FP32 is the vanilla GCN [7]. "FP32 (S)" refers to the PyG scatter-gather abstraction with maximal batch size. "FP32 (T)" refers to the PyG SpMM tensor abstraction. Bi-GCN [18] is the state-of-the-art binary GCN implementation. We compare the version that binarizes both activations and weights in the MM operation. "Ours (full)" refers to the *full-precision aggregation*, which is the same as in Bi-GCN. "Ours (bin)" refers to the *binary aggregation* version that uses MM.FBB + BSpMM.BBB for the first layer and MM.BBF + BSpMM.FBF for the second layer. "Peak Mem" refers to peak memory usage during inference. Acc refer to accuracy in percentage (%).

Dataset	Model	Peak Mem (B)	Acc (%)	End-to-end Time (ms)		
				GTX1080	TitanV	RTX3060Ti
Cora	FP32 (S) [7]	16.73M	81.4±0.4	1.25±0.01	0.91±0.03	1.00±0.01
	FP32 (T) [7]	16.73M	81.4±0.4	1.34±0.02	1.15±0.05	1.16±0.03
	Bi-GCN [18]	16.73M	81.2±0.8	1.84±0.04	1.91±0.02	1.57±0.02
	Ours (full)	1.37M	81.2±0.8	0.51±0.00	0.37±0.07	0.38±0.02
	Ours (bin)	0.73M	81.2±1.0	0.32±0.04	0.28±0.08	0.24±0.04
PubMed	FP32 (S)	48.71M	79.0±0.3	2.86±0.04	1.51±0.02	1.90±0.02
	FP32 (T)	48.71M	79.0±0.3	2.26±0.01	1.49±0.02	1.77±0.01
	Bi-GCN	48.71M	78.2±1.0	2.81±0.07	2.23±0.09	1.52±0.01
	Ours (full)	7.31M	78.2±1.0	2.29±0.05	0.84±0.05	1.14±0.00
	Ours (bin)	2.65M	78.1±1.1	0.74±0.04	0.33±0.05	0.44±0.01
CiteSeer	FP32 (S)	49.78M	70.9±0.5	2.60±0.03	1.43±0.04	1.74±0.01
	FP32 (T)	49.78M	70.9±0.5	2.70±0.01	1.56±0.01	1.88±0.05
	Bi-GCN	49.78M	68.8±0.9	2.44±0.00	2.22±0.04	1.33±0.09
	Ours (full)	2.56M	68.8±0.9	0.80±0.04	0.58±0.02	0.50±0.03
	Ours (bin)	1.77M	68.7±0.4	0.63±0.03	0.46±0.01	0.42±0.00

(bin). (iv) Because the previous binarized GNN (Bi-GCN) does not use a single bit but a word for a binarized value, it does not save space or time compared to the original full-precision GNNs. (v) Our more complete binarized version (*Ours (bin)*) achieves 2-3X extra space savings and 1.5-3X extra speedups than our version (*Ours (full)*) that uses full-precision aggregation, while the extra accuracy loss is only 0.1%. (vi) All those benefits are largely consistent across the datasets. One exception is the performance of *Ours (full)* on PubMed, where, *Ours (full)* shows insignificant speedups

on GTX1080 and RTX3060Ti than the original version while the *Ours (bin)* still shows substantial speedups. We attribute this to the relatively larger num_of_nodes that introduces large performance gaps between BSpMM.BBB and BSpMM.FBB for the first layer.

Inductive case: Tables 4 and 5 report the results of the three inductive GNNs on the two large datasets. The benefits are also significant in space and time, but there are some differences from those in the transductive case. We note the following points. (i) For inductive learning, the previous work [23] uses the F1-micro score rather than accuracy to measure the quality of the inferences. The F1-micro score is a combined metric of precision and recall [23, 42]. The binarization maintains most of the quality again, causing a 0.5–2.1% accuracy loss. (ii) The memory space savings are 1.72–16X. The savings are relatively modest than in the transductive case. The reason is that most of our space savings come from the bit representation of the values of the adjacency matrices and the node features. But the sparse representation also consists of indices of the non-empty tiles. Because most non-empty tiles contain only one non-zero value, we do not save much on the indexing data structures compared to the default CSR format. For the small graphs, the indexing data structures form only a small portion of the overall representation; but for large graphs, the portion becomes much larger. But the savings are still substantial. (iii) The speedups achieved by our versions are even more significant, ranging from 2X to 125X. The reason is that as the graphs become larger, the room for time savings also grows. Another benefit worth mentioning is that as the memory space usage is reduced substantially, the new method can load the entire graph into memory and produce the inferences of all the sampled subgraphs in one run, which can bring extra time savings than processing the subgraphs one by one.

Additionally, Table 4 shows a 4.1% accuracy loss on GraphSAGE-Reddit. We attribute this to the sensitivity of the originally-trained binary GraphSAGE and the small hidden size used. While the Reddit graph is significantly larger than Flickr, it only uses as few as 128 hidden nodes. Increasing the hidden nodes to 256 and 512 results in a smaller accuracy loss (~0.67%, ~0.9%). On Flickr, an 0.6% accuracy increase. GNN inference accuracy is unstable, especially on large graphs, which is not unique to GNNs. Studies have shown that a compressed DNN can sometimes achieve higher accuracy than the original. Our slight accuracy increase resulted from the binary aggregation approximation in the first GCN layer.

In Table 5, binary model inferences occasionally experience slowdowns due to (1) patterns of the two graphs (only one non-zero in most non-zero tiles) favor tensor kernel-based implementations. (2) Our GraphSaint uses some full-precision operations to maintain accuracy; (3) our implemented operators have some inefficiency on such graphs. More specifically, in multiplying a binary matrix with

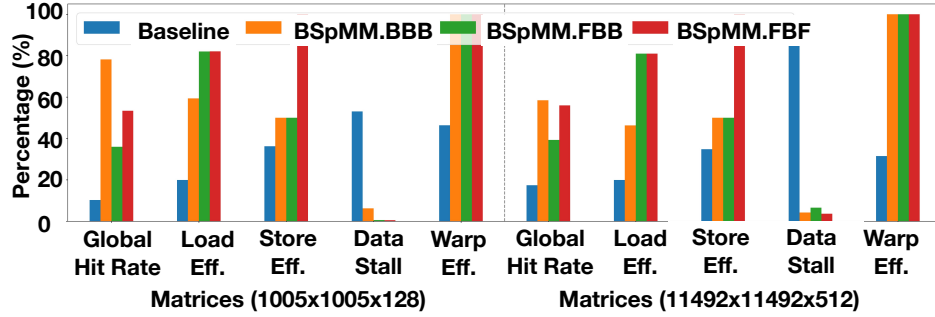


Figure 4: The profiling results of the multiplications of two pairs of representative sparse matrices using NSight on Nvidia GTX1080 GPU.

Table 4: Evaluation results of inductive GNNs – inductive GCN and GraphSAGE [23]. F1-micro is the metric to measure the accuracy of inductive GNNs. The *hidden size* is 256 for Flicker; 128 for Reddit. To avoid out-of-memory error, FP32 and Bi-GCN inferences are set to their maximal batch size on different GPUs.

Dataset	Model	Inductive GCN						Graph SAGE						
		Peak Mem (B)	F1-micro	End-to-end Time (s)			Peak Mem (B)	F1-micro	End-to-end Time (s)			GTX1080	TitanV	RTX3060Ti
				GTX1080	TitanV	RTX3060Ti			GTX1080	TitanV	RTX3060Ti			
Flicker	FP32 (S) [23]	358.07M	50.9±0.3	0.36±0.005	0.33±0.007	0.32±0.009	448.37M	50.9±1.0	0.36±0.006	0.32±0.004	0.32±0.008			
	FP32 (T) [23]	358.07M	50.9±0.3	0.045±0.000	0.035±0.000	0.03±0.000	448.37M	50.9±1.0	0.045±0.001	0.035±0.000	0.034±0.000			
	Bi-GCN [18]	358.07M	50.2±0.4	0.36±0.007	0.34±0.010	0.34±0.011	448.37M	50.2±0.4	0.36±0.008	0.33±0.003	0.33±0.002			
	Ours (full)	107.07M	50.2±0.4	0.023±0.01	0.016±0.000	0.02±0.003	196.9M	50.2±0.4	0.038±0.007	0.027±0.000	0.03±0.006			
	Ours (bin)	22.38M	49.9±0.3	0.006±0.004	0.002±0.000	0.005±0.000	27.52M	50.8±0.1	0.008±0.008	0.003±0.000	0.006±0.001			
	FP32 (S)	1.67G	93.3±0.0	49.01±0.25	38.19±0.10	38.70±0.28	1.81G	95.3±0.1	49.27±0.18	37.95±0.35	38.29±0.22			
Reddit	FP32 (T)	1.67G	93.3±0.0	0.86±0.02	0.45±0.001	0.52±0.007	1.81G	95.3±0.1	0.92±0.001	0.51±0.001	0.52±0.002			
	Bi-GCN	1.67G	93.1±0.2	49.30±0.28	38.22±0.10	38.97±0.34	1.81G	95.3±0.1	49.42±0.21	38.05±0.56	39.03±0.11			
	Ours (full)	1.02G	93.1±0.2	0.82±0.02	0.38±0.08	0.45±0.03	1.17G	95.3±0.1	0.90±0.003	0.45±0.03	0.53±0.04			
	Ours (bin)	943.77M	92.8±0.1	0.49±0.11	0.15±0.007	0.27±0.12	983.77M	91.2±1.2	0.53±0.05	0.20±0.009	0.29±0.05			

Table 5: Evaluation results of inductive GNNs – GraphSAINT [25, 26]. The *hidden size* is 256 for Flicker; 128 for Reddit.

Dataset	Model	Peak Mem (B)	F1-micro	End-to-end Time (s)		
				GTX1080	TitanV	RTX3060Ti
Flicker	FP32 (S) [25, 26]	623.72M	51.1±0.1	0.39±0.004	0.36±0.003	0.34±0.006
	FP32 (T) [25, 26]	623.72M	51.1±0.1	0.05±0.000	0.03±0.000	0.04±0.000
	Bi-GCN [18]	623.72M	50.8±0.2	0.05±0.003	0.04±0.000	0.04±0.001
	Ours (full)	371.83M	50.8±0.2	0.15±0.004	0.07±0.000	0.09±0.001
	Ours (bin)	202.39M	49.6±0.8	0.023±0.007	0.012±0.000	0.016±0.001
	FP32 (S)	2.04G	96.6±0.1	48.79±0.23	38.41±0.32	39.77±0.22
Reddit	FP32 (T)	2.04G	96.6±0.1	1.25±0.005	0.60±0.001	0.69±0.003
	Bi-GCN	2.04G	95.7±0.1	1.27±0.002	0.61±0.003	0.73±0.011
	Ours (full)	1.39G	95.7±0.1	0.92±0.46	0.66±0.08	0.74±0.08
	Ours (bin)	1.18G	94.5±0.6	0.45±0.16	0.24±0.003	0.33±0.09

a full-precision matrix, our implementation loads all full-precision elements corresponding to the entire tile. Such a strategy generally works fine but inefficiently for graphs of special patterns. We conditionally improve the implementation by loading only the elements corresponding to non-zero elements in the tile, seeing 2-3X speedups.

Hardware profiling: Using the GPU vendor’s profiling tool NSight, we find that the performance gain mainly originates from improved

memory utilization through binarization. Figure 4 shows the profiling results of three of our BSpMM kernels compared to the baseline—the default SpMM kernel in Torch Sparse when computing the multiplications of two pairs of representative matrices, measured on Nvidia GTX1080 GPU. Specifically, we observe significantly enhanced global load/store efficiency (from 19% to 80%), and L1/Tex cache hit rate (from 10% to 53-78%). In addition to that, with the data request stalls reduced from 53-89% to less than 10%, the warp execution efficiency surges from 31-46% to almost 100%.

Discussions: Regarding the overall number of operations to be executed, although BitGNN aggregates the multiply-accumulate operations of 32 elements into a single bit-dot-product operation upon one 32-bit operand, the actual reduction in operation count is less than 32X due to extra overhead on indexing. Nevertheless, since SpMM is typically memory-bound, binarization can still contribute to significant performance improvement.

The baselines reported in the comparisons use the classic scatter-gather form [43] in the implementation, as that is the common form in the original GNNs. An alternative (without using binarization) is in the form of sparse matrix multiplications [44]. We also experimented with the alternative form. For the transductive cases, that form brings no clear speedups. For Cora and CiteSeer, the alternative form actually causes 3-20% slowdowns over the scatter-gather form; for PubMed, there are slight speedups (1.01-1.62X). For the inductive cases, the alternative form is more efficient than the

scatter-gather form. But the BitGNN still shows clear benefits (e.g., 6-9X on Flickr), and the benefits of space remain as significant as before.

Potential impact: The reduced space and time brought by BitGNN not only improves the computing efficiency on server GPUs, but also opens new opportunities for dealing with large graphs (which cannot fit into memory) and for GNN to be used on resource-constrained devices. Quantized (non-GNN) deep neural networks have already been adopted in many domains on resource-constrained embedded scenarios, including auto-driving [45], smart agriculture [46], COVID19 face-cover detection [47], 3D object detection [48] and image processing [49]. This is mainly due to the simplified logic [50], low energy cost [51], low hardware requirement, and robustness [52]. Nevertheless, there are many scenarios the input data are non-Euclidean or can be better expressed by graphs, such as molecules [53], traffic flow [54], power-grid [55], etc. In these scenarios, the binary graph neural network, as a replacement of BNN, can play a vital role in feature extraction and real-time prediction.

5 RELATED WORKS

5.1 Binary Graph Neural Network

Binary GNNs recently emerged as a promising approach to applying quantization to graph learning workloads in the ML community. Up to now, although several works are proposing GNN binarization techniques and/or binary GNN models [18–21], none of them fulfill the performance advantages that can be achieved through the binarization, where BitGNN fills the void. Here, we summarize a few existing binary GNN studies.

Binary Graph Convolutional Network (Bi-GCN) [18] proposes a novel binary gradient approximation-based back-propagation technique for effectively training binary GCNs. It binarizes both the network parameters and node features with mere accuracy loss. Bi-GCN has been applied to both transductive-learning GNNs (e.g., GCN [7]) and inductive-learning GNNs (e.g., inductive-GCN, GraphSAGE [23] and GraphSAINT [25, 26]). Alternatively, Bahri et al. [19] employs knowledge distillation and multi-stage training to binarize the EdgeConv in Dynamic Graph CNNs (DGCNN) [5]. Wang et al. [20] propose a new binarized graph embedding method, named BGN, to binarize the parameters and pre-activations of Adaptive Sampling (AS-GCN) [56] and Graph Attention Network (GAT) [57]. In the back-propagation phase, they use two popular unbiased gradient estimators – the straight-through estimator and REINFORCE estimator [58], for binary approximation. Aside from XNOR and population count for +1 and -1 bit calculation, they involve masked summation and balance functions to improve the binarization process. Meta-Aggregator [21] introduces two aggregators – the Greedy Gumbel Aggregator (GNA) and Adaptable Hybrid Aggregator (ANA), aiming at enhancing the binary training accuracy during the aggregation phase.

These binarization techniques for GNNs provide a stepping stone in exploring the potential of binary GNNs. However, they only "logically" binarize GNN at the algorithm level; their implementations essentially use `sign()` and `mm()` in PyTorch. However, at the lower level, those GPU kernels still adopt full-precision tensors for storage and full-precision operations for computation. They did not showcase the performance potential of binary GNNs.

5.2 Bit-Manipulation on GPUs

Existing works have investigated the bit-operation capability of modern GPUs. The application scenarios span from image classification using CNNs [14, 28, 31, 59, 60], depth-sensing with stereo vision [45, 61], fraud detection [62], to graph algorithms [30].

Courbariaux et al. [14] first apply XOR and population-count operations to compute small MLPs on GPUs. Espresso [59] later implements a binary CNN library with C and CUDA backends, offering bit-packing and bit matrix multiplication functions. Khan et al. [60] extend the prior efforts of GEMM-based CNNs for real-time vehicle classification on desktop and embedded GPUs. BSTC [28] presents bit-block-based kernel designs for BMM and BConv, scaling the significant performance gains to deeper binary AlexNet, VGGNet, and ResNet. StereoBit [45] and FastFusion [61] develop the BNN-based stereo matching network with optimized implementation for reducing GPU on-chip memory footprint. They construct the network with binary feature descriptors for image pairs and weights, replacing expensive full-precision arithmetic operations with XOR and population count operations. Ye et al. [62] take advantage of the GPU intrinsics `_ballot_sync()`, `_match_any_sync()`, and `_popc()` to construct a Label Propagation (LP) algorithm for the fraud detection pipeline. Feng et al [63] decompose quantized neural network matrix multiplications into batches of BMM operations and rely on the Ampere tensorcores for acceleration. Finally, Bit-GraphBLAS [30] proposes a sparse bit storage format and a binary implementation of GraphBLAS operators for accelerating iteration-based graph algorithms when the graph edges are homogeneous that can be expressed as binary graphs.

These existing works present the performance optimization potential of leveraging bit manipulations and operations on GPUs. However, they are insufficient to handle the unique challenges (e.g., operator restructure, tensor representation, and inconsistent value multiplications) from binary GNNs.

6 CONCLUSION

BitGNN is the first work to fully exploit the design and challenges of realizing binary GNNs using bit tensors and bit manipulations. We propose a set of programming abstractions, tensor representation, and kernel design techniques to maximize the end-to-end binary GNN model performance. The optimizations and implementations provide an 8-22X end-to-end model acceleration to the prior binary GNN implementation.

ACKNOWLEDGEMENT

This material is based upon work supported by the U.S. Department of Energy, Office of Science, Office of Advanced Scientific Computing Research, ComPort: Rigorous Testing Methods to Safeguard Software Porting, under Award Number 78284. This material is also based upon work supported by the National Science Foundation (NSF) under Grant No. DE-EE0009357 and CNS-2107068. Any opinions, findings, and conclusions or recommendations expressed in this material are those of the authors and do not necessarily reflect the views of NSF or DOE.

REFERENCES

[1] Wenqi Fan, Yao Ma, Qing Li, Yuan He, Eric Zhao, Jiliang Tang, and Dawei Yin. Graph neural networks for social recommendation. In *The world wide web conference*, pages 417–426, 2019.

[2] Manon Réau, Nicolas Renaud, Li C Xue, and Alexandre MJJ Bonvin. Deeprank-gnn: a graph neural network framework to learn patterns in protein–protein interfaces. *Bioinformatics*, 39(1):btac759, 2023.

[3] Justin Gilmer, Samuel S Schoenholz, Patrick F Riley, Oriol Vinyals, and George E Dahl. Neural message passing for quantum chemistry. In *International conference on machine learning*, pages 1263–1272. PMLR, 2017.

[4] Hatem Helal, Jesun Firoz, Jenna Bilbrey, Mario Michael Krell, Tom Murray, Ang Li, Sotiris Xantheas, and Sutanay Choudhury. Extreme acceleration of graph neural network-based prediction models for quantum chemistry. *arXiv preprint arXiv:2211.13853*, 2022.

[5] Yue Wang, Yongbin Sun, Ziwei Liu, Sanjay E. Sarma, Michael M. Bronstein, and Justin M. Solomon. Dynamic graph cnn for learning on point clouds. *ACM Trans. Graph.*, 38(5), oct 2019.

[6] Jie-Fang Zhang and Zhengya Zhang. Point-x: A spatial-locality-aware architecture for energy-efficient graph-based point-cloud deep learning. In *MICRO-54: 54th Annual IEEE/ACM International Symposium on Microarchitecture*, page 1078–1090, New York, NY, USA, 2021. Association for Computing Machinery.

[7] Thomas N. Kipf and Max Welling. Semi-supervised classification with graph convolutional networks. In *International Conference on Learning Representations (ICLR)*, 2017.

[8] Liang Yao, Chengsheng Mao, and Yuan Luo. Graph convolutional networks for text classification. In *Proceedings of the AAAI conference on artificial intelligence*, volume 33, pages 7370–7377, 2019.

[9] Hongfan Ye, Buiqing Cao, Junjie Chen, Jianxun Liu, Yiping Wen, and Jinjun Chen. A web services classification method based on gcn. In *2019 IEEE Intl Conf on Parallel & Distributed Processing with Applications, Big Data & Cloud Computing, Sustainable Computing & Communications, Social Computing & Networking (ISPA/BDCloud/SocialCom/SustainCom)*, pages 1107–1114. IEEE, 2019.

[10] Jiali Liang, Yufan Deng, and Dan Zeng. A deep neural network combined cnn and gcn for remote sensing scene classification. *IEEE Journal of Selected Topics in Applied Earth Observations and Remote Sensing*, 13:4325–4338, 2020.

[11] Sheng Wan, Chen Gong, Ping Zhong, Shirui Pan, Guangyu Li, and Jian Yang. Hyperspectral image classification with context-aware dynamic graph convolutional network. *IEEE Transactions on Geoscience and Remote Sensing*, 59(1):597–612, 2020.

[12] Hao Jiang, Peng Cao, MingYi Xu, Jinzhu Yang, and Osmar Zaiane. Hi-gcn: A hierarchical graph convolution network for graph embedding learning of brain network and brain disorders prediction. *Computers in Biology and Medicine*, 127:104096, 2020.

[13] Itay Hubara, Matthieu Courbariaux, Daniel Soudry, Ran El-Yaniv, and Yoshua Bengio. Binarized neural networks. *Advances in neural information processing systems*, 29, 2016.

[14] Matthieu Courbariaux, Itay Hubara, Daniel Soudry, Ran El-Yaniv, and Yoshua Bengio. Binarized neural networks: Training deep neural networks with weights and activations constrained to +1 or -1. *arXiv preprint arXiv:1602.02830*, 2016.

[15] Mohammad Rastegari, Vicente Ordonez, Joseph Redmon, and Ali Farhadi. Xnor-net: Imagenet classification using binary convolutional neural networks. In *European conference on computer vision*, pages 525–542. Springer, 2016.

[16] Adrian Bulat and Georgios Tzimiropoulos. Xnor-net++: Improved binary neural networks. In *Proceedings of the British Machine Vision Conference (BMVC)*, 2019.

[17] Yichi Zhang, Zhiru Zhang, and Lukasz Lew. Pokebm: A binary pursuit of lightweight accuracy. In *Proceedings of the IEEE/CVF Conference on Computer Vision and Pattern Recognition*, pages 12475–12485, 2022.

[18] Junfu Wang, Yunhong Wang, Zhen Yang, Liang Yang, and Yuanfang Guo. Bi-gcn: Binary graph convolutional network. In *Proceedings of the IEEE/CVF Conference on Computer Vision and Pattern Recognition*, pages 1561–1570, 2021.

[19] Mehdi Bahri, Gaëtan Bahl, and Stefanos Zafeiriou. Binary graph neural networks. In *Proceedings of the IEEE/CVF Conference on Computer Vision and Pattern Recognition*, pages 9492–9501, 2021.

[20] Hanchen Wang, Defu Lian, Ying Zhang, Lu Qin, Xiangjian He, Yiguang Lin, and Xuemin Lin. Binarized graph neural network. *World Wide Web*, 24(3):825–848, 2021.

[21] Yongcheng Jing, Yiding Yang, Xinchao Wang, Mingli Song, and Dacheng Tao. Meta-aggregator: Learning to aggregate for 1-bit graph neural networks. In *Proceedings of the IEEE/CVF International Conference on Computer Vision*, pages 5301–5310, 2021.

[22] Matthias Fey and Jan E. Lenssen. Fast graph representation learning with PyTorch Geometric. In *ICLR Workshop on Representation Learning on Graphs and Manifolds*, 2019.

[23] William L Hamilton, Rex Ying, and Jure Leskovec. Inductive representation learning on large graphs. In *Proceedings of the 31st International Conference on Neural Information Processing Systems*, pages 1025–1035, 2017.

[24] Christopher Morris, Martin Ritzert, Matthias Fey, William L Hamilton, Jan Eric Lenssen, Gaurav Rattan, and Martin Grohe. Weisfeiler and leman go neural: Higher-order graph neural networks. In *Proceedings of the AAAI Conference on Artificial Intelligence*, volume 33, pages 4602–4609, 2019.

[25] Hanqing Zeng, Hongkuan Zhou, Ajitesh Srivastava, Rajgopal Kannan, and Viktor Prasanna. Accurate, efficient and scalable graph embedding. In *2019 IEEE International Parallel and Distributed Processing Symposium (IPDPS)*, May 2019.

[26] Hanqing Zeng, Hongkuan Zhou, Ajitesh Srivastava, Rajgopal Kannan, and Viktor Prasanna. Graphsaint: Graph sampling based inductive learning method. In *International Conference on Learning Representations*, 2020.

[27] Ang Li, Weifeng Liu, Linnan Wang, Kevin Barker, and Shuaiwen Leon Song. Warp-consolidation: A novel execution model for gpus. In *Proceedings of the 2018 International Conference on Supercomputing, ICS '18*, page 53–64, New York, NY, USA, 2018. Association for Computing Machinery.

[28] Ang Li, Tong Gen, Tianqi Wang, Martin Herbordt, Shuaiwen Leon Song, and Kevin Barker. Bstc: A novel binarized-soft-tensor-core design for accelerating bit-based approximated neural nets. In *Proceedings of the International Conference for High Performance Computing, Networking, Storage and Analysis, SC '19*, New York, NY, USA, 2019. Association for Computing Machinery.

[29] AMD. Hip programming guide: https://github.com/radeonopencompute/rocm/blob/rocm-4.5.2/amd_hip_programming_guide.pdf, 2022.

[30] Jou-An Chen, Hsin-Hsuan Sung, Xipeng Shen, Nathan Tallent, Kevin Barker, and Ang Li. Bit-graphblas: Bit-level optimizations of matrix-centric graph processing on gpu. In *2022 IEEE International Parallel and Distributed Processing Symposium (IPDPS)*, pages 515–525, 2022.

[31] Ang Li and Simon Su. Accelerating binarized neural networks via bit-tensor-cores in turing gpus. *IEEE Transactions on Parallel and Distributed Systems*, 32(7):1878–1891, 2020.

[32] Eli Ben-Sasson, Matan Hamilis, Mark Silberstein, and Eran Tromer. Fast multiplication in binary fields on gpus via register cache. In *Proceedings of the 2016 International Conference on Supercomputing*, pages 1–12, 2016.

[33] Guyu Huang, Guohao Dai, Yu Wang, and Huazhong Yang. Ge-spmm: General-purpose sparse matrix-matrix multiplication on gpus for graph neural networks. In *Proceedings of the International Conference for High Performance Computing, Networking, Storage and Analysis, SC '20*. IEEE Press, 2020.

[34] Md Rahman, Majedul Haque Sujon, Ariful Azad, et al. Fusedmm: A unified sddmm-spmm kernel for graph embedding and graph neural networks. In *35th Proceedings of IEEE IPDPS*, 2021.

[35] Technical report – bitgnn: Unleashing the performance potential of binary graph neural networks on gpus: <https://tinyurl.com/yuf87cax>, 2023.

[36] NVIDIA. Cuda programming guide, 2022.

[37] Yue Zhao, Jiaji Li, Chunhua Liao, and Xipeng Shen. Bridging the gap between deep learning and sparse matrix format selection. In *Proceedings of the 23rd ACM SIGPLAN Symposium on Principles and Practice of Parallel Programming*, 2018.

[38] Zhihui Yang, William Cohen, and Ruslan Salakhutdinov. Revisiting semi-supervised learning with graph embeddings. In *International conference on machine learning*, pages 40–48. PMLR, 2016.

[39] Weihua Hu, Matthias Fey, Marinka Zitnik, Yuxiao Dong, Hongyu Ren, Bowen Liu, Michele Catasta, and Jure Leskovec. Open graph benchmark: Datasets for machine learning on graphs. *Advances in neural information processing systems*, 33:22118–22133, 2020.

[40] Oleksandr Shchur, Maximilian Mumme, Aleksandar Bojchevski, and Stephan Günnemann. Pitfalls of graph neural network evaluation. *arXiv preprint arXiv:1811.05868*, 2018.

[41] Marinka Zitnik and Jure Leskovec. Predicting multicellular function through multi-layer tissue networks. *Bioinformatics*, 33(14):i190–i198, 2017.

[42] R. J. Fowlkes and D. G. Mallows. A method for comparing two hierarchical clusterings. *Journal of the American Statistical Association*, 78(383):553–569, 1983.

[43] F. Cucker and S. Smale. On the mathematical foundations of learning. *Journal of the ACM*, 52(5):607–627, 2005.

[44] Carl Yang, Aydin Buluç, and John D Owens. Design principles for sparse matrix multiplication on the gpu. In *European Conference on Parallel Processing*, pages 672–687. Springer, 2018.

[45] Gang Chen, Haitao Meng, Yucheng Liang, and Kai Huang. Gpu-accelerated real-time stereo estimation with binary neural network. *IEEE Transactions on Parallel and Distributed Systems*, 31(12):2896–2907, 2020.

[46] Chun-Hsian Huang. An fpga-based hardware/software design using binarized neural networks for agricultural applications: A case study. *IEEE Access*, 9:26523–26531, 2021.

[47] Nael Fasfous, Manoj-Rohit Vemparala, Alexander Frickenstein, Lukas Frickenstein, Mohamed Badawy, and Walter Stechele. Binarycop: Binary neural network-based covid-19 face-mask wear and positioning predictor on edge devices. In *2021 IEEE International Parallel and Distributed Processing Symposium Workshops (IPDPSW)*, pages 108–115. IEEE, 2021.

[48] Chao Ma, Yulan Guo, Yinjie Lei, and Wei An. Binary volumetric convolutional neural networks for 3-d object recognition. *IEEE Transactions on Instrumentation and Measurement*, 68(1):38–48, 2018.

[49] Yinglan Ma, Hongyu Xiong, Zhe Hu, and Lizhuang Ma. Efficient super resolution using binarized neural network. In *Proceedings of the IEEE/CVF Conference on Computer Vision and Pattern Recognition Workshops*, pages 0–0, 2019.

[50] Tong Geng, Tianqi Wang, Chunshu Wu, Chen Yang, Shuaiwen Leon Song, Ang Li, and Martin Herboldt. Lp-bnn: Ultra-low-latency bnn inference with layer parallelism. In *2019 IEEE 30th International Conference on Application-specific Systems, Architectures and Processors (ASAP)*, volume 2160, pages 9–16. IEEE, 2019.

[51] Tong Geng, Ang Li, Tianqi Wang, Chunshu Wu, Yanfei Li, Runbin Shi, Wei Wu, and Martin Herboldt. O3bnn-r: An out-of-order architecture for high-performance and regularized bnn inference. *IEEE Transactions on parallel and distributed systems*, 32(1):199–213, 2020.

[52] Angus Galloway, Graham W Taylor, and Medhat Moussa. Attacking binarized neural networks. *arXiv preprint arXiv:1711.00449*, 2017.

[53] Oliver Wieder, Stefan Kohlbacher, Mélaine Kuemann, Arthur Garon, Pierre Ducrot, Thomas Seidel, and Thierry Langer. A compact review of molecular property prediction with graph neural networks. *Drug Discovery Today: Technologies*, 37:1–12, 2020.

[54] Xiaoyang Wang, Yao Ma, Yiqi Wang, Wei Jin, Xin Wang, Jiliang Tang, Caiyan Jia, and Jian Yu. Traffic flow prediction via spatial temporal graph neural network. In *Proceedings of the web conference 2020*, pages 1082–1092, 2020.

[55] Christian Nauck, Michael Lindner, Konstantin Schürholt, Haoming Zhang, Paul Schultz, Jürgen Kurths, Ingrid Isenhardt, and Frank Hellmann. Predicting basin stability of power grids using graph neural networks. *New Journal of Physics*, 24(4):043041, 2022.

[56] Wenbing Huang, Tong Zhang, Yu Rong, and Junzhou Huang. Adaptive sampling towards fast graph representation learning. In S. Bengio, H. Wallach, H. Larochelle, K. Grauman, N. Cesa-Bianchi, and R. Garnett, editors, *Advances in Neural Information Processing Systems*, volume 31. Curran Associates, Inc., 2018.

[57] Petar Veličković, Guillem Cucurull, Arantxa Casanova, Adriana Romero, Pietro Liò, and Yoshua Bengio. Graph attention networks. In *International Conference on Learning Representations*, 2018.

[58] Ronald J Williams. Simple statistical gradient-following algorithms for connectionist reinforcement learning. *Machine learning*, 8(3):229–256, 1992.

[59] Fabrizio Pedersoli, George Tzanetakis, and Andrea Tagliasacchi. Espresso: Efficient forward propagation for binary deep neural networks. In *International Conference on Learning Representations*, 2018.

[60] Mir Khan, Heikki Huttunen, and Jani Boutellier. Binarized convolutional neural networks for efficient inference on gpus. In *2018 26th European Signal Processing Conference (EUSIPCO)*, pages 682–686. IEEE, 2018.

[61] Haitao Meng, Chonghao Zhong, Jianfeng Gu, and Gang Chen. A gpu-accelerated deep stereo-lidar fusion for real-time high-precision dense depth sensing. In *2021 Design, Automation & Test in Europe Conference & Exhibition (DATE)*, pages 523–528. IEEE, 2021.

[62] Chang Ye, Yuchen Li, Bingsheng He, Zhao Li, and Jianling Sun. *GPU-Accelerated Graph Label Propagation for Real-Time Fraud Detection*, page 2348–2356. Association for Computing Machinery, New York, NY, USA, 2021.

[63] Boyuan Feng, Yuke Wang, Tong Geng, Ang Li, and Yufei Ding. Apnn-tc: Accelerating arbitrary precision neural networks on ampere gpu tensor cores. In *Proceedings of the international conference for high performance computing, networking, storage and analysis*, pages 1–13, 2021.